Topography of Phase-Separated Critical and Off-Critical Polymer Mixtures

J. T. Cabral,[†] J. S. Higgins,*[,†] N. A. Yerina,[‡] and S. N. Magonov[‡]

Department of Chemical Engineering, Imperial College, London SW7 2BY, United Kingdom, and Digital Instruments/Veeco Metrology Group, 112, Robin Hill Rd., Santa Barbara, California 93117

Received August 20, 2001

ABSTRACT: We investigate the spinodal decomposition of a polymer mixture, at both critical and off-critical compositions, using atomic force microscopy. Phase separation in the bulk is imaged using tapping mode on the surface of microtomed samples. The generated surface profiles, revealed in height images, are analyzed according to their in-plane spinodal morphology and their (perpendicular) height distribution. The former is characterized in terms of the periodicity of the structure and volume fraction of coexisting phases, both in the percolation and cluster regimes. The average height profiles are shown to be bimodal with a height step, Δh, ranging from 1 to 7 nm, for the temperature quench depths spanned. Δh is time-independent but depends linearly on annealing temperature and therefore on the composition difference between coexisting phases. This temperature dependence allows us to extrapolate to the mixture's critical temperature. A blend of tetramethyl bisphenol A polycarbonate and polystyrene was employed for this demonstration.

I. Introduction

Real-space imaging of phase separation of polymer mixtures provides great insight into the resulting morphologies and has therefore attracted considerable interest. Early investigations include the pioneering transmission electron microscopy work by McMaster,[1] followed by a number of optical microscopy studies.[2,3] However, time-resolved scattering techniques (light, neutron, or X-ray) are more commonly employed since they provide *averaged* information about the structures. By effectively Fourier transforming the correlation function of spatial composition fluctuations,[4] the periodicity of the structure and the growth of fluctuation amplitudes are readily obtained. On the other hand, this statistical approach may fail to resolve structural details that are accessible to direct observation in real space. For example, different coarsening processes may yield identical scaling laws or a dominant demixing process may mask less prominent structures.[5,6] In addition, real-space imaging can directly quantify phase volume fractions or allow the computation of domain interface curvatures of various morphologies.[7]

There are several experimental techniques that probe phase separation in real space: optical microscopy (OM), transmission electron microscopy (TEM), and, more recently, atomic force microscopy (AFM), each characterized by a spatial window and resolution. OM (covering the micrometer to millimeter range) is well-suited for late stage coarsening studies, while TEM and AFM can explore the submicrometer range relevant to the earlier stages of phase separation. While microscopy offers direct qualitative insight, it requires Fourier analysis (of a *representative* sample region) to access global statistical information. It has two major drawbacks compared to scattering techniques: (i) it is usually not possible to perform real-time studies, and (ii) the focal depth may be too large compared to the structure of interest, thereby superposing information at different depths. The latter is largely eliminated by the use of laser scanning confocal microscopy (LSCM)[7−9] or by matching the specimen thickness to the relevant structure size (within 50−100 nm, for TEM[9]). AFM,[10] being mostly a surface technique, is not liable to such ambiguities since the experimental imaging conditions (low tip-force levels) can be tuned to restrict the penetration of the probe. There are no restrictions for AFM specimen thickness, and no labeling or staining is necessary, the only requirement being a dominant topography of interest compared to the surface noise. Furthermore, while low-force tapping is adequate for surface profiling, imaging at elevated forces can even provide near-surface compositional mapping. Also, the advent of AFM imaging at elevated temperatures allows in-situ monitoring of morphology changes at the surface, finding applications in melting and crystallization[11] and potentially in phase separation in thin films.

Numerous AFM investigations of phase separation of polymer mixtures have been reported over the past decade. Given the surface nature of the technique, these were invariably focused on thin or ultrathin films,[12−18] for which preferential surface wetting or confinement play a fundamental role and compete with phase separation dynamics. The combined processes result in surface undulations, resolvable by AFM, which are driven by surface tension modulations. However, we have recently extended the spectrum of AFM applications and reported, for the first time, on *bulk* phase separation of a polymer mixture.[19] Relatively thick films (about 100 μm) of a tetramethyl bisphenol A poly(carbonate)/poly(styrene) blend were isothermally annealed inside the thermodynamic unstable region, then quenched in the glassy state, and subsequently microtomed. The cross-sectional morphology revealed by AFM, with a roughness in the nanometer range, reproduced the expected spinodal structure revealed by optical microscopy. However, the structure factors obtained by time-resolved light scattering and by 2D-FFT of AFM images did not coincide, which was partially explained by geometric considerations about the dimen-

[†] Imperial College.
[‡] Digital Instruments/Veeco Metrology Group.

10.1021/ma0114990 CCC: $22.00
Published on Web 01/26/2002

sionality of the analysis involved. The generated topography was tentatively interpreted as due to a differential plastic deformation of the mixed phases occurring during fracture. The morphology at both interfaces (air and glass substrate) was also analyzed, revealing the interplay of spinodal decomposition and preferential attraction of blend components to lower interfacial energy surfaces.

We now extend this work to study phase separation of both critical and off-critical mixture of TMPC/PS, covering a wide range of temperature quench depths (up to 40 K) and annealing times. We have focused particularly on two aspects: (i) the phase separation mechanisms and kinetics, exploiting the wealth of detail provided by high-resolution real-space imaging (allowing, for example, the phase assignment and the determination of volume fractions or interfacial contour/area ratio); (ii) elucidating the nanometer scale topography, perpendicular to the surface, generated by controlled fracture (microtoming).

The article is organized as follows: Section II recalls phase separation fundamentals, in particular for off-critical blends, necessary to rationalize the morphologies obtained. The polymer mixture sample preparation, thermal treatment and microtoming, and atomic force microscopy measurements are described in section III. In section IV, we present and discuss the experimental results obtained for near-critical and off-critical blends in terms of (i) in-plane bulk morphologies and (ii) height profiles. We determine the characteristic sizes of the spinodal structure, via 2D-FFT of AFM topography images, as a function of annealing time and temperature and show that the height profiles exhibit two clear plateaus, corresponding to the two coexisting phases. The height separation between these plateaus, which is in the nanometer range, depends solely on the composition difference between the phases and thus vanishes near the critical point. Section V summarizes these findings.

II. Phase Separation

A binary mixture at equilibrium quenched into another homogeneous, but nonequilibrium, state inside its phase boundary can take two phase separation pathways to approach thermodynamic equilibrium.[20] Spinodal decomposition (SD) occurs inside the spinodal line, where the system is unstable toward fluctuations of infinitesimal amplitude. The metastable state (between the spinodal and binodal lines) is characterized by instability to fluctuations of large enough amplitude, leading to a decay by droplet nucleation and growth (NG).

Independent of the phase separation mechanism, a polymer mixture of composition ϕ annealed inside the phase boundary will demix into two coexistent phases with the compositions, ϕ' and ϕ'', such that the overall free energy is minimized. Their volume fractions, f' and f'' (with $f' + f'' = 1$), are obtained by a conservation equation:

$$\phi = f'\phi' + (1 - f')\phi'' \tag{1}$$

yielding

$$f' = 1 - f'' = \frac{\phi - \phi''}{\phi' - \phi''} \tag{2}$$

Knowledge of the phase diagram and of the initial composition ϕ determines all ϕ', ϕ'', f' and f'' at any given temperature. The ratio between volume fractions, which can be directly obtained in real-space imaging, has repercussions for how the phase-separated structures evolve with time.

Since all experimental results reported here concern rapid quenches inside the spinodal boundary, we shall concentrate only on SD kinetics and coarsening mechanisms.

A. Early Stage.[21] Spontaneous long-wavelength fluctuations, randomly oriented in space, drive the initial decay of the unstable state. The amplitude of such fluctuations grows exponentially, formally corresponding to a negative diffusion coefficient. The amplification factor (or growth rate), $R(\Lambda)$, depends on the fluctuation wavelength and has a time-independent maximum at Λ_m, defining a *characteristic size* of the structure. The resulting morphology is the well-known bicontinuous, interpenetrating, spinodal structure.

This onset of SD is well described by the linearized theory of Cahn−Hilliard. At later times, when equilibrium compositions are reached, growth slows down and the excess free energy at the interfaces drives the coarsening of the structures.

B. Coarsening[20,22] reduces the interfacial area per unit volume by smoothing the interfaces and merging phase-separated domains. The kinetics of the process is characterized by the time, t, evolution of Λ_m, the composition fluctuation wavelength of maximum amplitude. The early stage is followed by a crossover time domain, during which both the wavelength and the amplitude of the fluctuations grow. In the late stages,[23] equilibrium compositions are attained, and the coexisting phases are separated by sharp interfaces. The spinodal structure grows self-similarly, obeying simple scaling laws:[24]

$$\Lambda_m \propto t^{\alpha} \tag{3}$$

A number of coarsening mechanisms are relevant, each associated with a power law exponent:

$$\alpha \approx \begin{cases} 1/3 & \text{evaporation−condensation} \\ 1/3 & \text{Brownian coalescence} \\ 1 & \text{hydrodynamic flow} \end{cases} \tag{4}$$

The evaporation−condensation (or Ostwald ripening) mechanism corresponds to the growth of large droplets at the expense of small ones, which involves chain diffusion through the opposite phase. It was first derived by Lifshitz−Slyozov[25] to account for the limiting case of a small minority phase ($f' \gg f''$) structure. Brownian coalescence is the usual random diffusion and merging of spherical droplets. Both *diffusion* processes yield a similar $\alpha = 1/3$ dependence, making them indistinguishable when observed from the time dependence of Λ_m. Siggia[26] showed that hydrodynamic flow, driven by excess surface tension of connected droplets, could decrease the average curvature of a structure, leading to domain growth. This fast process (characterized by $\alpha = 1$) dominates the coarsening of percolated structures, while slower diffusion mechanisms drive coarsening of cluster morphologies.

C. Critical and Off-Critical Quenches. The domain structure and growth kinetics depend on the volume fraction ratio of the coexistent phases. A mixture with $f' \approx f''$ remains percolated until late stages of

phase separation, while if $f' \gg f''$ the continuity of the minority phase is rapidly lost, resulting in a dispersed droplet/matrix morphology. Consequently, given the different mechanisms involved, critical mixtures coarsen faster than off-critical ones.[27]

In general, a near-critical spinodal morphology coarsens following a sequence of steps: (i) an initial transient regime after the early stage, (ii) diffusive growth at intermediate times ($\alpha = 1/3$), followed by a (iii) crossover to $\alpha = 1$ at longer times, when hydrodynamic effects become important. The structure remains interconnected until very late stages.

The first stages of off-critical coarsening (i−iii) are, in principle, identical to those described above. However, hydrodynamic flow is only effective while the structure is bicontinuous. As the percolated SD structure breaks up, slower droplet growth kinetics ($\alpha = 1/3$) takes over (iv), giving rise to a second crossover. The overall off-critical behavior is somewhat complex and depends strongly upon the structure connectivity (and, hence, on f'/f''). One should always bear in mind that, when comparing off-critical coarsening kinetics at different temperature quenches, ΔT, one is actually dealing with different f'/f'' ratios—the shallower the quench, the more asymmetric the volume fractions (according to eq 2). Simultaneously, the driving force for phase separation increases with ΔT.

The asymptotic $1/3$ power law is commonly observed for off-critical quenches.[5,28,29] However, careful light scattering experiments by Takeno and Hashimoto[29] have identified the scaling sequence $\alpha \approx 1 \rightarrow 1/3$, referred to as percolation-to-cluster transition (PCT), at certain volume fractions and quench depths. Entering the cluster regime, coarsening slows down so severely[30] that the structures were initially reported to be pinned.[31,32] The authors have also shown, for both an UCST[31] and a LCST[29] mixture, that the deeper the quench depth, the later PCT occurs and the larger the characteristic structure size at which it takes place. This is consistent with the above discussion of how f'/f'' depends on ΔT.

Furthermore, it has recently been reported[5,6] that during the PCT (the second kinetic crossover) percolated and cluster morphologies coexist. The process was observed by microscopy and light scattering and yields a structure factor with two maxima, corresponding to two characteristic lengths. Because of their different topology, the structures grow with different scaling laws, which has allowed their deconvolution: while the percolated morphology follows $\alpha = 1$, the dispersed phase grows with a slower $\alpha = 1/3$. These results indicate that the crossover from percolated to dispersed morphology is heterogeneous.

III. Experimental Section

A. Materials. Blends of tetramethyl bisphenol A polycarbonate (TMPC) and polystyrene (PS) were prepared by solution casting onto glass slides. TMPC ($M_W = 5.4 \times 10^4$ g/mol, PDI = 3.5, $T_g = 197$ °C) was obtained from Bayer and PS ($M_W = 22.5 \times 10^4$ g/mol, PDI = 2.2, $T_g = 102$ °C[33]) from BP Chemicals; tetrahydrofuran (10% w/v solutions) was chosen as common solvent. The films were dried for 2 days in air and then for 4 weeks under vacuum (10^{-1} mbar) at gradually increasing temperatures, finally above the blend $T_{g,blend}$, resulting in thickness of about 100 μm. Two model compositions were studied: near-critical TMPC/PS 50/50 and off-critical 70/30 (w/w).

TMPC/PS was chosen for this study because it exhibits lower critical solution temperature (LCST) phase behavior and has both critical point ($T_C \approx 235$ °C) and $T_{g,blend}$ above room temperature: $T_C > T_{g,blend} >$ RT. This is particularly convenient, since the phase-separated morphologies can be arrested at any time by quenching to room temperature. The mixture's phase diagram has been published elsewhere.[34] Further, TMPC/PS is a highly interacting blend, which implies large driving forces for phase separation even at shallow quenches and results in fast coarsening.[34d]

Samples were isothermally annealed in a vacuum oven at temperatures above the phase boundary for different time intervals, ranging from 50 to 1000 s, and then quenched to RT (which is, at least, 100 °C below the blend $T_{g,blend}$). The annealing temperatures were measured by a thermocouple placed in contact with the sample holder. A large temperature range was investigated—from 240 °C, just above the phase boundary, to 275 °C. This ensures that the resulting compositions will range from rather similar, after a shallow quench (for which $\Delta\phi = |\phi' - \phi''|$ is small), to very dissimilar after a deep quench (large $\Delta\phi$). Both 50/50 and 70/30 compositions fall inside the spinodal region for all temperatures studied,[34] which becomes evident from the morphologies reported below. Varying annealing time allows the phase-separated domains to relax their shape, coalesce, and grow larger. Varying the annealing temperature has various repercussions: it (i) tunes the composition of the resulting phases while (ii) changing the rate of domain coarsening and (iii) the f'/f'' ratio for off-critical quenches. The annealing temperature and time were kept below 280 °C[35] and 1000 s to keep polymer degradation to a minimum.

Each phase-separated film was peeled from the substrate, mounted on a substrate, and microtomed along its cross section with a diamond knife (both Micro Star Technologies, TX) at room temperature. Sample cutting was performed at 0.5 mm/min, at an angle of 49°. Often, specimens had to be microtomed several times before the surface noise (including knife marks and chattering features) could be kept under 1 nm (rms).

B. Atomic Force Microscopy. A scanning probe microscope MultiMode Nanoscope IIIA (Digital Instruments, Santa Barbara, CA), operating in tapping mode, at ambient conditions, was employed in this study. Conventional etched Si probes (stiffness ~ 40 N/m, resonant frequency 160−170 kHz) were used; the amplitude of the free-oscillating probe, A_0, was varied in the 10−20 nm range while the set-point amplitude, A_{sp}, ranged from 0.5 to 0.8 A_0. Varying the tip−force range is essential to unambiguously determine the surface topography.[10,36,37] Contact mode measurements, which are characterized by stronger tip−sample forces, were performed to confirm absolute height profiles.

The analysis presented is fundamentally based on height images. Where available, phase images generally coincide with topography patterns obtained from height images, confirming the domain and volume fraction assignments. However, these often could not be obtained since, given the high sensitivity of phase response, minute surface imperfections cause loss of phase contrast coherence, especially when imaging large surface areas (hundreds of μm^2).

The characteristic wavelength of the spinodal structures, at various annealing temperatures and times, was deduced from radially averaged power spectra obtained by 2D fast Fourier transform (FFT) of the height images. Height distributions (perpendicular to the microtomed surface) were also obtained from the topography. The results and error bars presented summarize data from at least four images, of various scan sizes and from different sample regions, to minimize local sampling artifacts. A diagram of the setup used, showing the sample cross section and relevant imaging axes, is given in Figure 1.

IV. Results and Discussion

The presentation of results is organized as follows. First, (A) we describe how the bulk morphology coarsens with time for a near-critical and an off-critical composition at various quenches depths. In section B, the issue of the composition of the phases, left unanswered in our

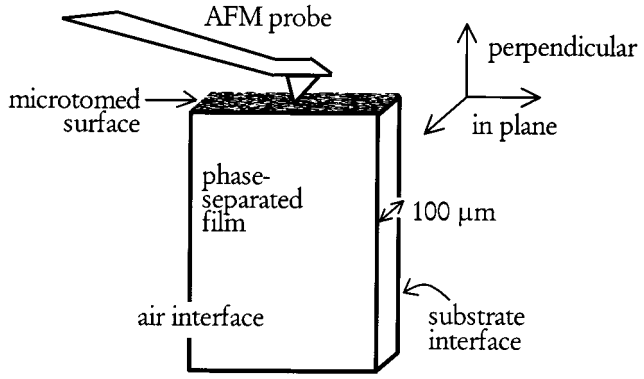

Figure 1. Schematic of the sample geometry and imaging setup used. A phase-separated film (about 100 μm thick) is mounted on a holder and cross-sectioned. The resulting topography is imaged with AFM tapping mode and interpreted in terms of the *in-plane* morphology and (*perpendicular*) height distribution. The air and glass (substrate) interfaces are also indicated.

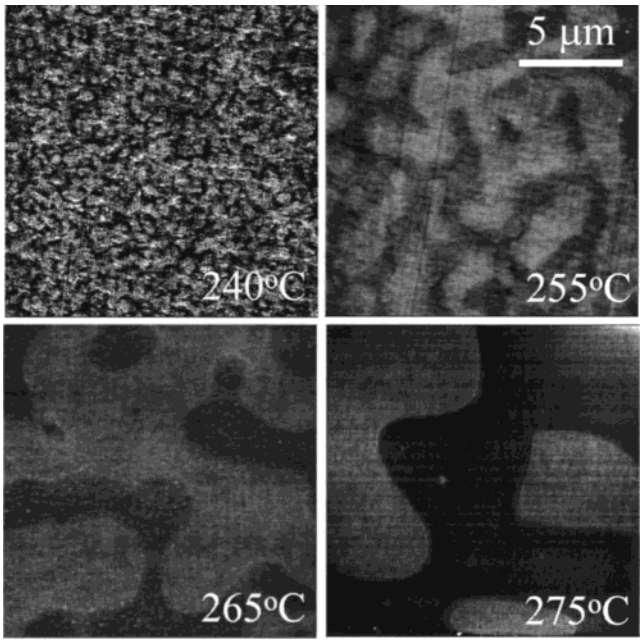

Figure 2. Spinodal decomposition of a near-critical mixture, TMPC/PS 50/50, at various temperatures for a constant time (500 s). AFM topography (15 × 15 μm^2 scans) of microtomed surfaces. Two height scales (25 nm for images at 240 and 255 °C and 50 nm for 265 and 275 °C) were employed to better display the morphologies.

previous report,[19] is addressed in a number of ways. In particular, we compute average height distributions (perpendicular to the microtomed surface) and rationalize the obtained bimodal profiles. In section C we discuss the origin of this height contrast.

A. Bulk Morphology. Films of near-critical composition TMPC/PS 50/50 were isothermally annealed at various temperatures and subsequently microtomed at room temperature. The generated surface topography was imaged in tapping mode. Typical results are presented in Figure 2: AFM height images (15 × 15 μm^2 scans) of samples annealed at 240, 255, 265, and 275 °C for 500 s. Note that the compositions of the phases (ϕ' and ϕ'') on each image are different, as defined by the phase diagram and quench depth, ΔT. A light/dark color corresponds to high/low topography, as conventionally used, and the height range is given for each image. The corresponding structure factors, characterizing the in-plane periodicity, were determined by 2D-FFT of the height images. The time evolution of the power spectra obtained for a rather deep quench (~20 °C inside the spinodal) is shown in Figure 3. Note the logarithmic spatial scale, covering 20 nm−65 μm. The position of the peak maximum defines Λ_m, the wavelength of dominant compositions fluctuations, which is taken as the *characteristic size* of the structure. These measurements complement our previous report,[19] enlarging the temperature quench depth and annealing time ranges.

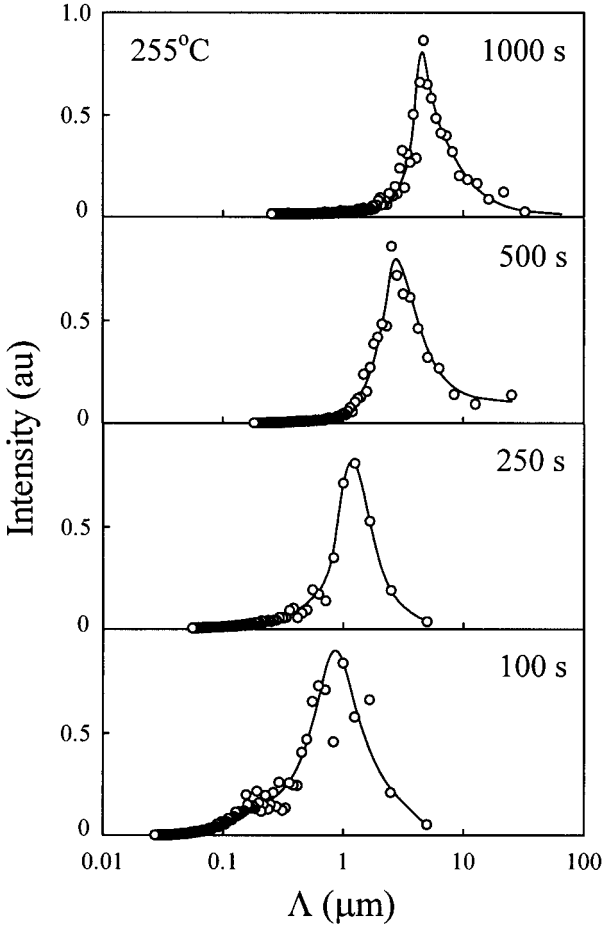

Figure 3. Power spectra of spinodal decomposition of a near-critical mixture TMPC/PS 50/50 annealed at 255 °C for varying times; results obtained from 2D-FFT of scans of dimensions ranging from 5 × 5 to 65 × 65 μm^2. Note the logarithmic spatial axis, spanning 0.020−65 μm.

Figure 4 compiles the results obtained for the near-critical blend TMPC/PS 50/50 into a coarsening map: Λ_m is represented as a function of temperature (240−275 °C) and time (0−1000 s). The straight lines indicate a $\Lambda_m \propto t^1$ dependence, characteristic of hydrodynamic-driven coarsening. The inset of the figure shows the earlier states of phase separation, in the submicron range, which should obey slower kinetics.

Coarsening scattering data are frequently represented in reduced plots,[20b] where the characteristic wavenumber $q_m(t)$ is rescaled by its initial value $q_m(0)$ and represented against a reduced time $\tau = tD_{app}q^2_m(0)$; D_{app} is the apparent (or mutual) diffusion coefficient, obtained from the exponential amplitude growth during the early stages, and $q_m = 2\pi/\Lambda_m$. Both $q_m(0)$ and D_{app} are quench depth-dependent (both increasing with ΔT).[20] However, because each AFM structure factor is obtained from a different sample, it was not possible to

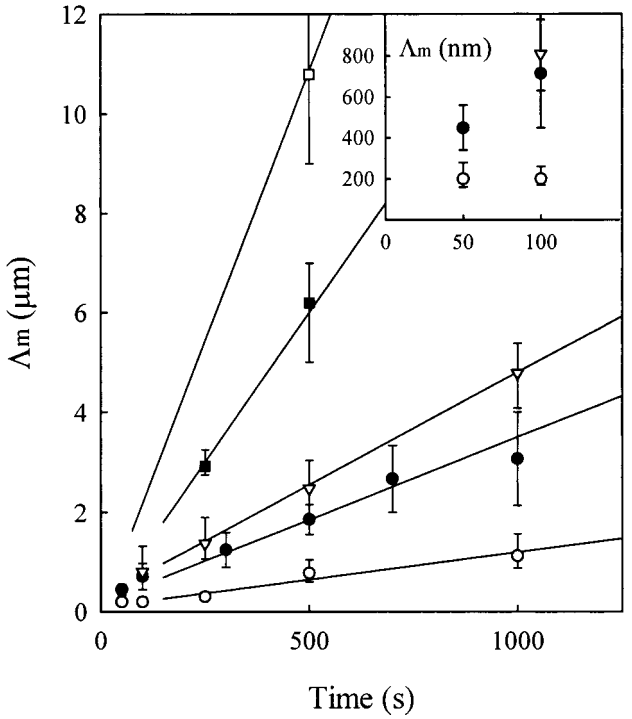

Figure 4. Coarsening dynamics of TMPC/PS 50/50. Time−temperature map defining the wavelength of maximum amplitude fluctuation, Λ_m, at (○) 240, (●) 245,[19] (▽) 255, (■) 265, and (□) 275 °C. The error bars are estimated from scans of various dimensions and from the inherent breadth of the structural maximum. Straight lines indicate hydrodynamic coarsening, following $\alpha = 1$. The inset shows in greater detail the onset of phase separation, obeying to slower diffusive kinetics.

perform a growth rate analysis. This is a common drawback of real-space techniques, in particular at early stages of phase separation, during which surface noise is relatively important compared to the coherent phase separation morphology.[24]

Next we report, for the first time using AFM, on spinodal decomposition of an off-critical mixture. Figure 5 shows topographic data of TMPC/PS 70/30 mixtures after a very shallow temperature quench (240 °C) following annealing times of 100, 250, 500, and 1000 s. The observed morphology is qualitatively similar to that obtained for a near-critical 50/50 quench at the same temperature in the early times (Figure 9a, after 100 s annealing time), which evolves into the commonly observed bicontinuous structure (Figure 2a, after 500 s). This initial spinodal morphology is clearly distinguishable from that originated by a nucleation and growth process.[38] The corresponding (submicrometer) power spectra are presented in Figure 6. While the structure factors obtained after deep quenches or long annealing times (see Figure 3) conform to an expected Lorentzian shape,[23] such shallow quenches (Figure 6) produce rather asymmetric profiles. We believe this is due to long wavelength noise induced by the cross-sectioning of the samples (knife marks and residual chattering); when the height contrast between the phases is small, noise becomes relatively important.

Figure 7 illustrates the coarsening of a spinodal morphology of an off-critical mixture after a deep temperature quench (at 265 °C). Even at the earliest time shown (250 s), the spinodal structure is not fully percolated, although the minority phase keeps some degree of continuity. This morphology relaxes quickly,

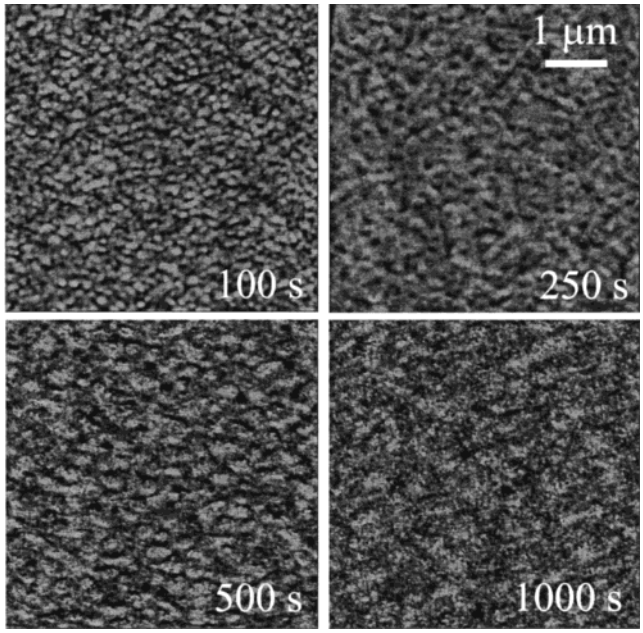

Figure 5. AFM topography of an off-critical mixture, TMPC/PS 70/30, undergoing spinodal decomposition after a shallow quench (at 240 °C). 5×5 μm^2 scans of microtomed surfaces, with 15 nm height range.

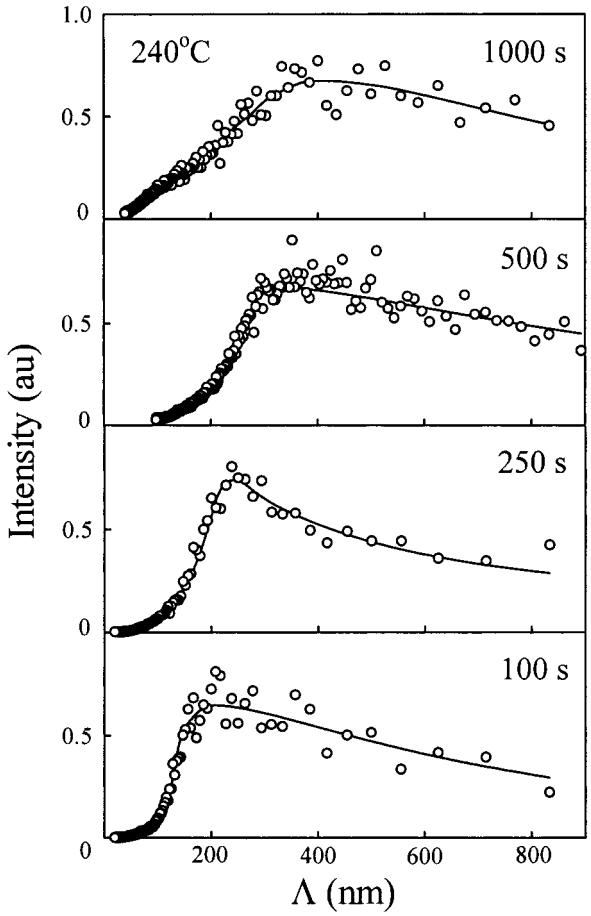

Figure 6. Power spectra obtained from 2D-FFT and radial averaging of the previous images (Figure 5) of an off-critical TMPC/PS 70/30 blend annealed at 240 °C. Note the suitability of the AFM spatial window (down to 20 nm in these spectra) to resolve the earlier stages of phase separation. Lines are guides to the eyes.

reducing the average curvature with time. At the latest time, the continuity of the domains is lost, giving rise

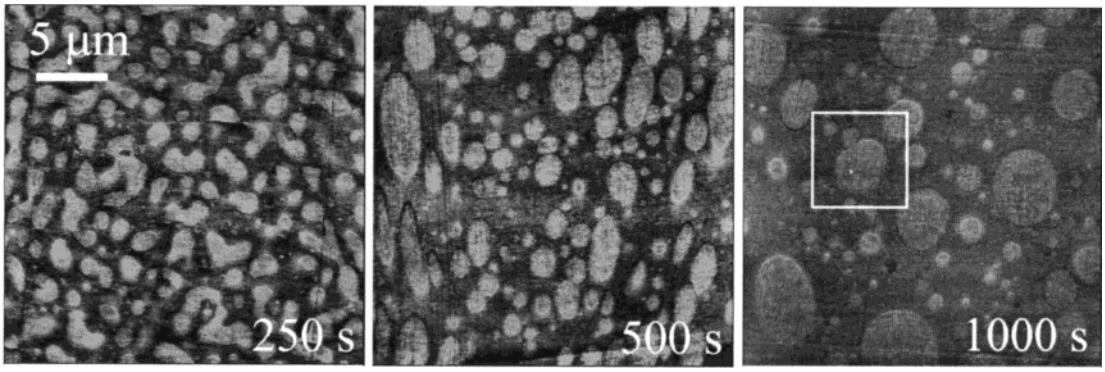

Figure 7. Coarsening of an off-critical blend, TMPC/PS 70/30, annealed at 265 °C (a deep quench) imaged by 25 × 25 μm^2 topography scans with 30 nm height range. The initial connectivity of the structure is a signature of spinodal decomposition, while the disproportionate volume fractions of the two phases is characteristic of an off-critical mixture. Coarsening is fast, and the domain shapes relax into large droplets within short time.

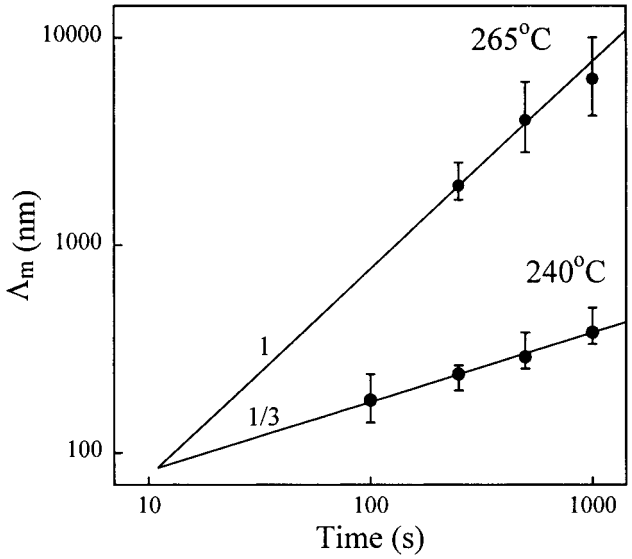

Figure 8. Coarsening dynamics of off-critical TMPC/PS 70/30 after isothermal annealing at 240 and 265 °C, inside the unstable region of the phase diagram. After the shallow quench, the structure grows diffusively, following $\alpha = 1/3$. Hydrodynamic flow ($\alpha = 1$) dominates coarsening after the deep temperature quench (lines are guides to the eyes).

to a rather polydisperse droplet distribution where diameters of over 5 μm and under 200 nm coexist. This morphology crossover, discussed in section IIC, is known as percolation-to-cluster transition and is in striking contrast with the near-critical behavior, for which continuity is preserved until late stages (Figure 2).

The coarsening kinetics of both deep and shallow off-critical quenches are presented in Figure 8, where power spectrum maxima are shown as a function of time. The quench at 240 °C exhibits a $t^{1/3}$ dependence characteristic of a diffusion-dominated process, expected during intermediate stages of phase separation. After a deep temperature quench, at 265 °C (about 30 deg inside the spinodal), the spinodal structure coarsens following t^1, a scaling characteristic of hydrodynamic flow. However, a direct inspection of the images shows that, while the reduced domain curvature could be accounted for by this mechanism, the volume increase of the minority domains should involve a second (diffusive) process, as expected from a crossover in coarsening dynamics. The sequence of images—locally connected precipitates evolving toward spherical growing droplets—indicates that PCT occurs during the observed time window. The sample annealed for 1000 s suggests that Brownian

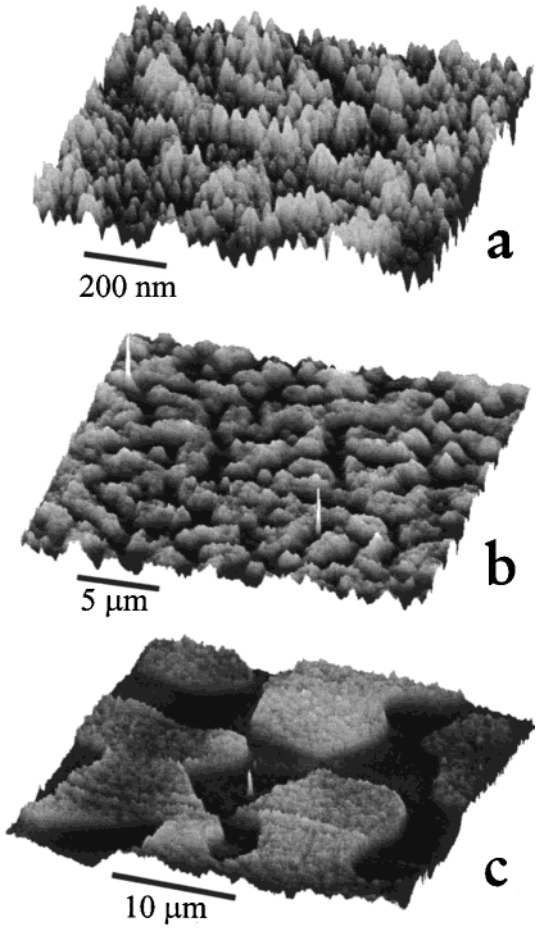

Figure 9. AFM topography of representative stages of spinodal decomposition of the near-critical blend TMPC/PS 50/50: (a) 1 μm scan of a sample annealed for 100 s at 240 °C (a shallow quench)—early stage, exhibiting a granular structure defining a fine periodicity; (b) sample annealed for 500 s at 255 °C—late stage coarsening, with sharp interfaces and well-defined composition plateaus; (c) sample annealed for 500 s at 275 °C—the latest stage imaged, retaining however the domain connectivity. These height profiles are quantitatively analyzed in Figure 10.

coalescence (indicated by the square in Figure 7) could also play a role at this temperature, which is probably not surprising, given the low viscosities (of a few hundreds of Pa s, as estimated from the WLF relationship for PS[39]). Finally, the resulting volume fractions are rather similar after the shallow quench ($f' \approx f''$) while very asymmetric after the deep quench ($f'/f'' \approx$

1.8), in agreement with the expected off-critical behavior presented in section IIC.

A final word concerns the coarsening dynamics probed in 2 and 3 dimensions. We have recently shown,[19] on geometrical grounds, that considerable shifts of the structural periodicity obtained from a 2D image could be expected during the early stages of phase separation. However, as the structure factor sharpens, these become limited, and consequently, the coarsening laws should follow the same power laws ($\alpha = 1$ and $^1/_3$) as in 3D, with the absolute values of Λ_m being shifted by about 5% (beyond our current resolution). These results generally agree with the present findings. However, the limited data available in the earlier stages of phase separation do not allow us to probe such dynamics, which are expected to differ considerably from the linear regime ($\Lambda_m \propto t^0$) observable with scattering (3D) techniques.

Overall, Figures 2−4 generally demonstrate the remarkable *spatial window* of the technique, capable of resolving structures from about 10 nm to 100 μm, encompassing the relevant length scales of phase separation. Figures 5 and 6 illustrate the *resolution* of the measurements, only limited by intrinsic surface noise. AFM imaging combines an unmatched dynamic range of $\Lambda_{max}/\Lambda_{min} > 250$ for a single measurement (compared to 20−50 for SANS or LS) along with an overall ratio of about 10^4, with nanometer resolution, combining scans of different sizes.

B. Phase Assignment by Height Distribution. In our first report of bulk phase separation using AFM,[19] we had not been able to assign the composition of the phases. We now solve the issue in several ways. A straightforward way of determining which phase is richer in which blend component is by analyzing off-critical mixtures, for which the resulting volume fractions are asymmetrical. A phase-separated blend of TMPC/PS 70/30 is expected to have a minority phase richer in PS and a TMPC-rich matrix. From Figure 7, the higher phase emerges as being PS rich.

Measurements on a near-critical mixture provide another route. After imaging a microtomed surface of a deeply phase-separated sample (TMPC/PS 50/50 265 °C for 250 s), the sample was annealed for 2 h at the glass transition temperature of the original mixed blend (135 °C). AFM imaging performed in the same region revealed that, while the low phase was unaltered, the topography of the higher phase had changed, and the (inevitable) light microtoming scratches had disappeared. Again, the high phase is identified as having a lower $T_{g,blend}$ and hence being polystyrene rich.

It would, however, be useful to explore quantitative tools to map compositions of heterogeneous materials. In the following, we address this question using average height distributions *perpendicular* to the surface (rather than *in-plane*, used to characterize the bulk spinodal structure), which are obtained by averaging the 3D surface profile of phase-separated blends. We report separately on how nanoindentation can contribute to this issue.[38]

Figure 9 presents the coarsening of the near-critical composition TMPC/PS 50/50 at various representative stages. Apart from the scaling of the morphology, the images have a different *absolute* height difference between the two phases. This is explored quantitatively in Figure 10a, where the average height distribution is plotted for various temperatures (after 500 s annealing

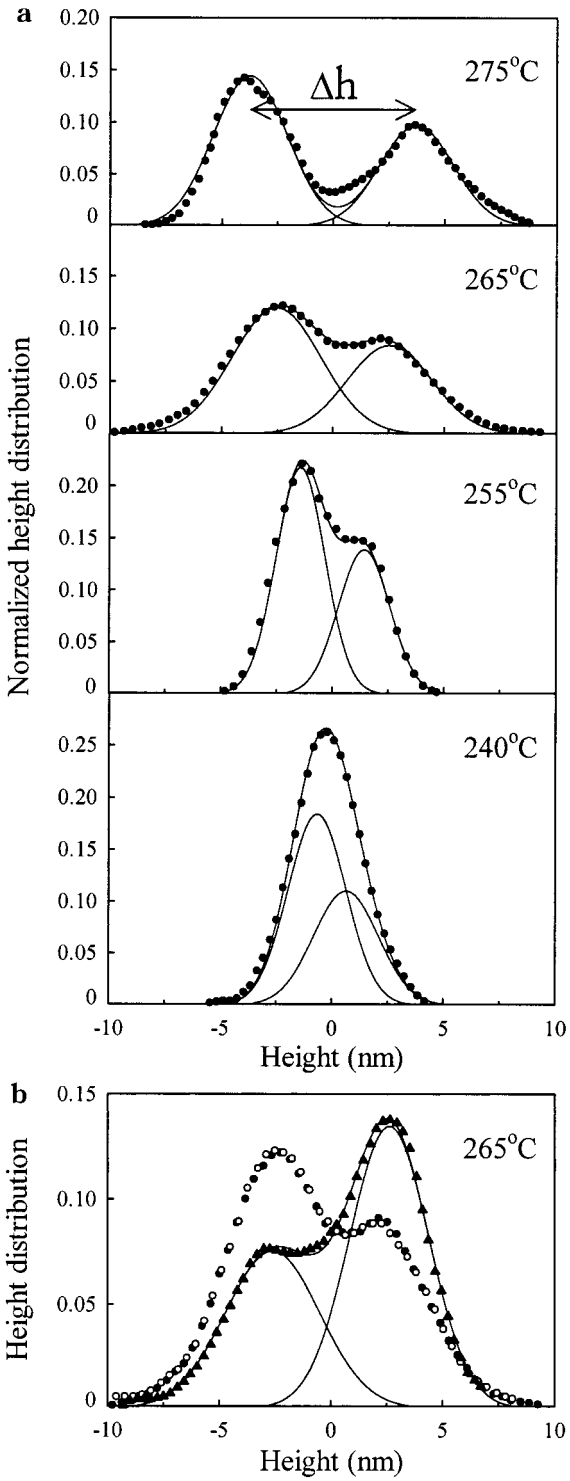

Figure 10. (a) Average height distributions (perpendicular to surface) of the topography scans obtained for TMPC/PS 50/50 after annealing at the indicated temperatures for 500 s; (●) experimental data. The bimodal profiles are deconvoluted with a simple normalized double-Gaussian distribution; the center of the distribution is fixed at zero height. The phase above the mean surface level, identified as PS-rich, is represented with negative height; the low phase, TMPC-rich, appears with positive height. **(**b**)** Average height profile of microtomed surfaces. TMPC/PS 50/50 blends quenched at 265 °C for (○) 250 s and (●) 500 s (same as (a)), showing that the profile does not depend on annealing time. (▲) TMPC/PS 70/30 annealed at the same temperature (for 250 s) and double-Gaussian fit. These results show that the height profiles, in particular the distance between maxima, Δh, depends only on the annealing temperature and, hence, on the composition difference between phases.

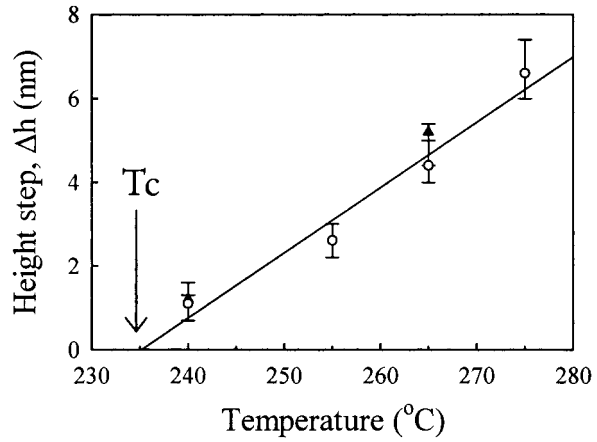

Figure 11. Height step, Δh, dependence with phase separation temperature for (○) TMPC/PS 50/50 and (▲) 70/30. The line, extrapolating to $\Delta h \rightarrow 0$, is a guide to the eyes. Deep quenches result in coexisting phases of very different composition and hence, in large height steps; the shallower the quench, the smaller Δh, vanishing at the critical point ($T_C \approx 235$ °C).

time). The profiles clearly show two peaks, whose height difference depends on the annealing temperature. The center of the distribution was (arbitrarily) set to height = 0, with the high phase (PS-rich) represented as negative and the low phase (TMPC-rich) as positive. The experimental data (circles) were fitted to normalized double-Gaussian distributions:

$$g(h) = f'G(h_0',\sigma') + f''G(h_0'',\sigma'') \qquad (5)$$

where G is a Gaussian function; h_0 and σ are respectively its mean value and standard deviation. The prefactors f' and f'' obey to $f' + f'' = 1$ and are interpreted as the volume fractions of the coexisting phases. This is equivalent to computing the relative areas of the "high" and "low" phases by direct inspection of the images. All the profiles at this composition could be well described by $f' \equiv f_{PS-rich} = 0.6$ and $f'' \equiv f_{TMPC-rich} = 0.4$, in very good agreement with the computed values from the phase diagram.[34,38]

Furthermore, the height profiles were shown to be annealing time *independent*. This is illustrated in Figure 10b where we plot the results obtained for TMPC/PS 50/50 annealed at 265 °C for 250 s (○) and 500 s (●), during which the characteristic size, Λ_m, doubles. The bimodal fit is not shown for simplicity. In the same figure we represent the off-critical profile (▲) obtained at the same temperature. Two features are noticeable: (i) the height step between phases is approximately the same while (ii) the volume fraction of the phases has appreciably changed ($f_{PS-rich} = 0.35$ and $f_{TMPC-rich} = 0.65$), in accordance with the phase diagram for this quench depth.

We have now shown that the average height step, Δh, depends on annealing temperature but not on annealing time for both near-critical and off-critical mixtures. This implies that Δh is determined by the *composition difference* of the phases $\Delta\phi = |\phi' - \phi''|$. With this idea in mind, we plot Δh against annealing temperature in Figure 11 and find a linear dependence, within error bars. The height contrast vanishes at about 235 °C, which agrees well with T_C, the critical temperature of the mixture, at which $\phi' \approx \phi''$. The height step mimics the composition difference and appears therefore to follow

$$\Delta h \propto \Delta T \propto \Delta\phi \qquad (6)$$

The last proportionality holds as long as the temperature range is sufficiently far from the critical point.[40] (Otherwise, a quadratic-like dependence can be computed from the experimental phase diagram.) The overall validity of our reasoning depends, however, on the relevant mechanical property of the mixtures being *additive* (a weighted average of that of pure polymers), which we have tested employing nanoindentation.[38] Moreover, the proportionality constant (K_f) relating Δh to $\Delta\phi$ is likely to depend on the fracture conditions.

The width of individual Gaussians ($\sigma \approx 1.5$) does not change appreciably with temperature, and this smearing of the height levels is thought to be a function of the fracture conditions. This explains why the bimodal profile at the lowest temperature investigated (where the compositions are most similar) is rather convoluted and suggests a limitation of this analysis toward very shallow temperature quenches (but not to earlier stages of phase separation after *deep* quenches).

A final remark concerns the absolute values of the height step, Δh. In AFM imaging of heterogeneous polymer systems, such as blends and block copolymers, the apparent topography revealed in tapping mode height images is known to depend on tip−force conditions.[36,37] This occurs mostly when one component is glassy and the other rubbery-like, at the temperature the measurements are carried out.

We have therefore imaged the phase-separated samples using various tip−force levels in tapping mode and performed control measurements in contact mode. These generally confirmed Δh to span 1−7 nm, depending on quench depth. Consequently, the height distance between the two phases is effectively *smaller* than the unperturbed radius of gyration of the polymers (about 13 nm for PS[41]).

C. Origin of Height Contrast. In our previous report, we had tentatively interpreted the height contrast between the phases as due to a different extent of nonreversible (plastic) deformation experienced during fracture (or microtoming). We can now provide supporting evidence for this assumption. Although both TMPC and PS are rather brittle at room temperature, the latter is more ductile and should therefore undergo larger deformation before failure.[38] Accordingly, the PS-rich phase appears consistently at a higher topography than the TMPC-rich one (section IVB). Further, when the composition difference disappears, the contrast vanishes.

All cross-sectioned surfaces presented here were consistently obtained by diamond-knife, room temperature microtoming. We expect that fracture conditions will have important repercussions on the resulting topography, namely on Δh. These should be included in the proportionality constant of eq 5. For example, decreasing the microtoming temperature should reduce the height contrast, as the fracture behavior becomes increasingly brittle.[42] However, in a number of systems examined (TMPC/PS, PS/PVME, and PMMA/SMA[38]), tuning the cross-sectioning conditions, while keeping coherent phase contrast larger than surface noise, has proven to be a laborious task.

V. Summary

We examine bulk spinodal decomposition of a near-critical and an off-critical TMPC/PS mixture. Phase

separation was induced by isothermal annealing at various temperatures within 240−275 °C and annealing times up to 1000 s. Samples were then cross-sectioned with a diamond knife at room temperature and imaged using atomic force microscopy. The resulting structure periodicities, Λ_m, ranging between 200 nm and 12 μm, were obtained from 2D-FFT of AFM images.

Average height profiles are shown to be bimodal and annealing-temperature-dependent but time-independent. These are well-described by normalized double-Gaussian distributions. The separation between the two deconvoluted maxima defines a height step between the coexistent phases, Δh, which ranges between 1 and 7 nm. This separation between the two topographic plateaus (which is smaller than R_g) is argued to be a function of the composition difference between coexisting phases and therefore vanishes at the critical point. The perspective of direct compositional mapping appears encouraging, given the drawbacks involved in determining phase compositions with other techniques: cloud point measurements inevitably fall in the metastable region, small-angle scattering requires demanding intensity calibrations, and calorimetry does not yield structural information. A differential plastic deformation between domains of slightly different composition is reiterated as the mechanism responsible for the topographic contrast.

The procedure described provides a route to generate controlled surface morphologies (percolated or droplet/matrix), in both the surface plane and height. The former is tuned according to phase separation kinetics while the latter depends on phase composition differences and/or fracture conditions. This effort joins a number of recent studies[43−45] aimed at controlling the surface topographies of polymer blends via phase separation.

Acknowledgment. J.T.C. acknowledges the financial support from Fundação para a Ciência e Tecnologia, Portugal, and Digital Instruments, Santa Barbara, for hospitality.

References and Notes

(1) McMaster, L. P. *Adv. Chem. Ser.* **1975**, *142*, 43.
(2) Nishi, T.; Wang, T. T.; Kwei, T. K. *Macromolecules* **1975**, *8*, 227.
(3) Strobl, G. R.; Bendler, J. T.; Kambour, R. P.; Shultz, A. R. *Macromolecules* **1986**, *19*, 2683.
(4) Higgins, J. S.; Benoît, H. C. *Polymers and Neutron Scattering*; Clarendon Press: Oxford, 1994.
(5) Okada, M.; Sun, J.; Tao, J.; Chiba, T.; Nose, T. *Macromolecules* **1995**, *28*, 7514.
(6) Takeno, H.; Nakamura, E.; Hashimoto, T. *J. Chem. Phys.* **1999**, *110*, 3620.
(7) Jinnai, H.; Koga, T.; Nishikawa, Y.; Hashimoto, T.; Hyde, S. T. *Phys. Rev. Lett.* **1997**, *78*, 2248.
(8) Jinnai, H.; Nishikawa, Y.; Koga, T.; Hashimoto, T. *Macromolecules* **1995**, *28*, 4782.
(9) Ribbe, A. E.; Hashimoto, T. *Macromolecules* **1997**, *30*, 3999.
(10) Recent reviews on AFM in polymer science: (a) Magonov, S. N.; Reneker, D. *Annu. Rev. Mater. Sci.* **1997**, *27*, 175. (b) *Scanning Probe Microscopy of Polymers*; Ratner, B., Tsukruk, V. V., Eds.; ACS Symposium Series; American Chemical Society: Washington, DC, 1998; p 694. (c) Magonov, S. N. In *Encyclopedia of Analytical Chemistry*; Meyers, R. A., Ed.; John Wiley & Sons Ltd.: Chichester, 2000; p 7432.
(11) Godovsky, Y. K.; Magonov, S. N. *Langmuir* **2000**, *16*, 3549. Ivanov, D. A.; Amalou, Z.; Magonov, S. N. *Macromolecules* **2001**, *34*, 8944.
(12) Saraf, R. F. *Macromolecules* **1993**, *26*, 3623.
(13) Tanaka, K.; Yoon, J.-S.; Takahara, A.; Kajiyama, T. *Macromolecules* **1995**, *28*, 934.
(14) Ermi, B. D.; Karim, A.; Douglas, J. F. *J. Polym. Sci., Polym. Phys. Ed.* **1998**, *36*, 191.
(15) Karim, A.; Slawecki, T. M.; Kumar, S. K.; Douglas, J. F.; Satija, S. K.; Han, C. C.; Russell, T. P.; Liu, Y.; Overney, R.; Sokolov, J.; Rafailovich, M. H. *Macromolecules* **1998**, *31*, 857.
(16) Heier, J.; Kramer, E. J.; Revesz, P.; Battistig, G.; Bates, F. S. *Macromolecules* **1999**, *32*, 3758.
(17) Newby, B. Z.; Composto, R. J. *Macromolecules* **2000**, *33*, 3274.
(18) Müller-Buschbaum, P.; Gutmann, J. S.; Stamm, M. *Macromolecules* **2000**, *33*, 4886.
(19) Cabral, J. T.; Higgins, J. S.; McLeish, T. C. B.; Strausser, S.; Magonov, S. N. *Macromolecules* **2001** *34*, 3748.
(20) Comprehensive reviews on phase separation: (a) Gunton, J. D.; San-Miguel, M.; Sahni, P. S. In *Phase Transitions and Critical Phenomena*; Domb, C., Lebowitz, J. L., Eds.; Academic: New York, 1983; Vol. 8, p 267. In particular for polymer blends: Hashimoto, T. *Phase Transitions* **1988**, *12*, 47.
(21) (a) Cahn, J. W. *J. Chem. Phys.* **1965**, *42*, 93. (b) de Gennes, P.-G. *J. Chem. Phys.* **1980**, *72*, 4756. (c) Pincus, P. *J. Chem. Phys.* **1981**, *75*, 1996. (d) Binder, K. *J. Chem. Phys.* **1983**, *79*, 6387.
(22) Doi, M. In *Theoretical Challenges in the Dynamics of Complex Fluids*; McLeish, T. C. B., Ed.; NATO ASI Series, Series E: Applied Sciences; Kluwer Academic: Dordrecht, 1997; Vol. 339, p 293.
(23) Furukawa, H. *Adv. Phys.* **1985**, *34*, 703.
(24) Both the periodicity Λ_m and the amplitude of composition fluctuations obey scaling laws in the intermediate and late stages. We have, however, based our analysis solely on $\Lambda_m(t)$, since absolute intensities for the structure factors could not be accurately extracted from different AFM images of cross-sectioned samples. This is particularly significant for the earlier stages of phase separation, for which the coherent topography is most affected by surface noise. For this reason, a linearized dynamic analysis of the early stages, yielding growth rates, $R(\Lambda)$, and necessary to reduce the coarsening data to a master curve, was not carried out.
(25) Lifshitz, I. M.; Slyozov, V. V. *J. Phys. Chem. Solids* **1961** *19*, 35.
(26) Siggia, E. D. *Phys. Rev. A* **1979**, *20*, 595.
(27) We loosely use the terminology critical and off-critical with the meaning of quenches yielding similar and dissimilar volume fractions. This is nevertheless valid for TMPC/PS since the mixture exhibits a rather symmetric phase diagram (ref 34).
(28) Sung, L.; Han, C. C. *J. Polym. Sci., Polym. Phys. Ed.* **1995**, *33*, 2405.
(29) Takeno, H.; Hashimoto, T. *J. Chem. Phys.* **1997**, *107*, 1634.
(30) Crist, B. *Macromolecules* **1996**, *29*, 7276.
(31) Hashimoto, T.; Takenaka, M.; Izumitani, T. *J. Chem. Phys.* **1992**, *97*, 679.
(32) Läuger, J.; Lay, R.; Gronski, W. *J. Chem. Phys.* **1994**, *101*, 7181.
(33) M_W and PDI are the weight-average molecular weight and polydispersity index, respectively; T_g is the glass transition temperature, measured by differential scanning calorimetry (DSC) at 10 °C/min.
(34) (a) Guo, W.; Higgins, J. S. *Polymer* **1990**, *31*, 699. (b) Kim, E.; Kramer, E. J.; Osby, J. O.; Walsh, D. J. *J. Polym. Sci., Polym. Phys. Ed.* **1995**, *33*, 467. (c) Merfeld, G. D.; Paul, D. R. *Polymer* **2000**, *41*, 649. (d) Cabral, J. T.; Gerard, H.; Higgins, J. S., to be submitted to *J. Chem. Phys.*
(35) Hellmann, E. H.; Hellmann, G. P.; Rennie, A. R. *Colloid Polym. Sci.* **1991**, *269*, 343.
(36) Magonov, S. N.; Cleveland, J.; Elings, V.; Denley, R.; Whangbo, M.-H. *Surf. Sci.* **1997**, *85*, 201.
(37) Knoll, A.; Margerle, R.; Krausch, G. *Macromolecules* **2001** *34*, 4159.
(38) Cabral et al., manuscript in preparation.
(39) Extrapolated using the Williams−Landel−Ferry (WLF) equation $\log[\eta(T)/\eta(T_g)] = [-C_1(T - T_g)]/[C_2 + (T - T_g)]$, with parameters $C_1 = 16.35$ and $C_2 = 52.5$ (from: Ngai, K. L.; Plazek, D. J. In *Physical Properties Handbook*; Mark, J. E., Ed.; American Institute of Physics: Woodbury, NY, 1996) for the relevant M_w.
(40) Stockmayer, W. H.; Solc, K.; Lipson, J. E. G.; Koningsveld, R. In *Contemporary Topics in Polymer Science*; Culbertson, B. M., Ed.; Plenum Press: New York, 1989.
(41) Calculated for polystyrene using the empirical relation between the radius of gyration and molecular weight (or segment length), $R_g = 0.27M_W^{1/2}$, yielding $R_g \approx 13$ nm for

the M_W used (after: Boothroyd, A. T.; Rennie, A. R.; Wignall, G. D. *J. Chem. Phys.* **1993**, *99*, 9135).
(42) Kinloch, A. J.; Young, R. J. *Fracture Behaviour in Polymers*; Chapman and Hall: London, 1983.
(43) Böltau, M.; Walheim, S.; Mlynek, J.; Krausch, G.; Steiner, U. *Nature (London)* **1998**, *391*, 877.
(44) Nisato, G.; Ermi, B. D.; Douglas, J. F.; Karim, A. *Macromolecules* **1999**, *32*, 2356.
(45) Higgins, A. M.; Jones, R. A. L. *Nature (London)* **2000**, *404*, 476.

MA0114990